



CHORUS

This is the accepted manuscript made available via CHORUS. The article has been published as:

Magnetic and electrical transport properties of $\text{YbFe}_{2}\text{O}_{4}$

R. C. Rai, J. Hinz, D. Mckenna, J. Pawlak, and M. DeMarco

Phys. Rev. B **100**, 045102 — Published 2 July 2019

DOI: [10.1103/PhysRevB.100.045102](https://doi.org/10.1103/PhysRevB.100.045102)

Magnetic and electrical transport properties of YbFe_2O_4

R. C. Rai,* J. Hinz, D. Mckenna, J. Pawlak, and M. DeMarco
Department of Physics, SUNY Buffalo State, Buffalo, NY 14222, USA
(Dated: June 17, 2019)

We present magnetic and electrical transport properties such as resistivity, magnetoresistance, dielectric, and polarization of polycrystalline YbFe_2O_4 . The ferrimagnetic transition temperature is measured at 243 K, followed by the two low-temperature transitions at ~ 190 K and ~ 65 K, respectively. The magnetic properties including the M-H hysteresis loops exhibit a strong temperature dependence and possibly indicate a spin-glass state below 65 K for YbFe_2O_4 . The iron Mössbauer measurement at 295 K confirms the presence of two Fe sites. The measured resistivity can be modeled with the Mott's variable-range hopping model, $\rho \propto \exp(T_0/T)^{1/4}$, indicating the electron hopping between Fe^{2+} and Fe^{3+} sites. The magnetoresistance effects up to 6% at 8 T were observed and the effects could be caused by the field-induced changes in the electron hopping processes. The frequency-dependent complex dielectric constant has been found to be strongly influenced by the contact effects, and the polarization of [polycrystalline](#) YbFe_2O_4 does not show ferroelectricity.

I. INTRODUCTION

Multiferroics demonstrate a peculiar cross-coupling between two ferroic states, such as ferromagnetic and ferroelectric properties, leading to interesting physics as well as potential technological applications.¹⁻³ YbFe_2O_4 (YbFO hereafter), which is isostructural to LuFe_2O_4 (LFO), belongs to the rare-earth oxide family RFe_2O_4 ($\text{R} = \text{Y, Dy to Lu}$) with mixed-valence ions of Fe^{2+} and Fe^{3+} in the hexagonal lattice, resulting in spin and charge frustrations in the system.⁴⁻⁸ As a result, this family of oxides exhibit a series of magnetic transitions and the charge-ordering phenomenon. In particular, YbFO goes through a spin-glass transition below ~ 80 K, a ferrimagnetic transition at ~ 245 K, and a three-dimensional charge ordering (CO) transition at ~ 300 K.⁹⁻¹⁴

The family of RFe_2O_4 attracted attention after Ikeda et al. first reported that LFO is a high temperature ($T_N \sim 240$ K) multiferroic in which the electrical polarization was interpreted as the CO induced phenomenon.^{4,6,15} However, the subsequent studies by other researchers found that the colossal dielectric property and ferroelectricity of LFO were strongly influenced by the extrinsic effects, not driven by the anticipated CO mechanism.¹⁶⁻²⁰ Hearmon et al. have studied YbFO using synchrotron x-ray diffraction and found a frustration-driven incommensurate CO transition at 320 K.²¹ The results of the neutron diffraction experiments on stoichiometric YbFO showed a three-dimensional CO transition between 390 K and 440 K and T_N at 245 K.¹⁴ Furthermore, the previously reported ferrimagnetic to antiferromagnetic transition at ~ 175 K in LFO was not observed in YbFO . Recently, Nagata et al. have reported the direct observation of the electric polarization in single crystal YbFO with a relatively weak electric remnant polarization value of 1 nC/cm².²² Therefore, YbFO is still a potential candidate for multiferroicity and it is an interesting system. The focus of research on YbFO is to explore both complex magnetic states and electrical polarization and whether it is a multiferroic material.

In this paper, we report on structural, resistivity, mag-

netoresistance, electrical polarization, magnetic, and dielectric properties of polycrystalline YbFO . The x-ray diffraction pattern show a single phase YbFO with a small amount of impurities. The room temperature Mössbauer spectrum indicates the presence of Fe^{2+} and Fe^{3+} states in the sample. We present the magnetic moment versus temperature and magnetic field for YbFO which show a ferrimagnetic transition at $T_N = 243$ K, followed by the two low temperature transitions at $T^* \sim 190$ K and $T^{**} \sim 65$ K. Further, the magnetic data point to a complex magnetic state below 65 K, and we discuss the role of the Yb ions and their interactions with the Fe ions for the low temperature magnetic state. The resistivity of YbFO can be explained by the Mott's variable-range hopping model of the form $\rho \propto \exp(T_0/T)^{1/4}$. We also present the dielectric properties of a polycrystalline YbFO sample between 100 K and 350 K, which exhibit a typical low-frequency behavior dominated by the extrinsic effects. Finally, we present the electrical polarization data that do not display polarization-field loops as expected from a ferroelectric material.

II. EXPERIMENTAL

YbFO samples were prepared by an electron-beam assisted solid state reaction. The detail sample preparation can be found in our earlier work on LFO.²³ Here, we briefly describe the important steps. A stoichiometric ratio of Yb_2O_3 and Fe_2O_3 powder samples were thoroughly mixed and ground, followed by pelletizing and sintering at 1200 °C for 12 hours in air. The processes were repeated one more time and the sample was sintered at 1200 °C for 15 hours. Then, the sintered pellet was heated by an electron-beam (ebeam) gun in the vacuum chamber with the oxygen partial pressure of $\sim 5 \times 10^{-4}$ Torr. The pellet was heated slowly by gradually increasing the ebeam power. In particular, we monitored the temperature of the pellet by watching the color of the pellet and the evaporation rate on the quartz-crystal film thickness monitor. The ebeam power was adjusted

to give a constant evaporation rate on the monitor. After heating the pellet continuously for more than 30 minutes, the pellet slowly started melting. We continuously heated the pellet until the top surface of the pellet was completely melted, and then the ebeam power was gradually decreased to zero within five to ten minutes. The top surface of YbFO appears shiny with polycrystalline images [as shown in Fig. 1 (a)]. After removing from the ebeam chamber, the YbFO pellet was annealed in a muffle furnace at 600 °C in air.

For dielectric and polarization measurements, a polycrystalline sample with dimensions 3 mm x 2 mm x 0.9 mm was polished on both sides and copper wires were attached with silver paste in the parallel plate capacitor geometry. Polarization was measured between 20 K and room temperature using Premier II Ferroelectric Tester (Radiant Technologies) while dielectric properties were measured in the frequency range 500 Hz - 1 MHz between 100 K and 350 K using QuadTech 1920 LCR Meter. Rigaku MiniFlex 600 diffractometer with the Cu K_{α} source ($\lambda = 1.54 \text{ \AA}$) was used for x-ray diffraction (xrd) characterization. Similarly, the magnetic moment as a function of temperature (4 - 350 K) and the magnetic moment versus magnetic field (up to 8 Tesla) hysteresis loops were measured on a 20 mg polycrystalline YbFO using Vibrating Sample Magnetometer option of Physical Property Measurement System (PPMS), Quantum Design. Furthermore, the Electrical Transport Option of PPMS was used to measure resistivity and magnetoresistance utilizing a 4-probe technique with silver paste as the electrical contacts. The same bulk polycrystalline YbFO sample was used for the dielectric, electrical transport, and magnetic properties measurements. We also measured ^{57}Fe Mössbauer spectrum at room temperature. The xrd and Mössbauer measurements were done on the powder samples.

III. RESULTS AND DISCUSSION

Figure 1(a) from left to right shows a YbFO pellet at three different stages of the synthesis process: a freshly pressed sample (left), a sample sintered at 1200°C (middle), and a polycrystalline sample (right). As shown, the polycrystal YbFO sample has a shiny surface with multiple crystals having a few millimeters in dimensions. Figure 1(b) shows the xrd pattern of the YbFO powder sample, prepared by an ebeam assisted method. The xrd pattern shows strong intensities from the (003), (006), (101), and (009) planes of YbFO, consistent with the hexagonal lattice of YbFO.²⁴ Similarly, the signals from other planes of YbFO are also present. In addition, the weak signals from impurity phases, Fe_2O_3 (denoted by *) at 49.4°, 54.5°, 57.7° and orthorhombic YbFeO_3 (denoted by +) at 23.3°, 26.2°, and 34.3°, respectively, are also observed.^{25,26} The weak intensities of these impurity peaks suggest that the amount of impurities is reasonably low. Thus, the xrd pattern shows a single phase YbFO

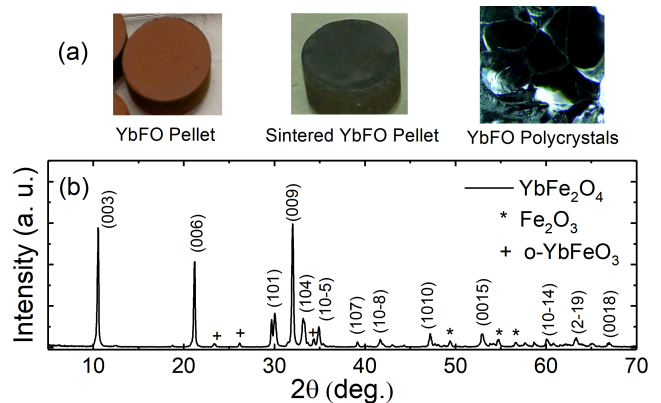


FIG. 1. (a) Images of YbFO pellets representing three different stages of the synthesis process: (left to right) a freshly pressed sample, a sample sintered at 1200°C, and a polycrystalline sample prepared by an ebeam-assisted method. (b) The xrd pattern of the YbFO powder sample, showing intense signals from the (003), (006), and (009) planes and other planes. The weak signals from impurity phases Fe_2O_3 and orthorhombic YbFeO_3 (denoted by * and +) are also observed.

sample with a small amount of impurities.

Figure 2(a) shows the magnetic moment as a function of temperature for a 20 mg polycrystalline YbFO pellet for zero-field cooling (ZFC) and field cooling (FC) at $H = 1 \text{ kOe}$. The ferrimagnetic transition temperature is observed at $T_N = 243 \text{ K}$, followed by two low temperature transitions at $T^* \sim 190 \text{ K}$ and $T^{**} \sim 65 \text{ K}$, respectively. These transition temperatures were extracted from the derivative of the ZFC curve. The measured ferrimagnetic transition temperature $T_N = 243 \text{ K}$ is close to the reported value of $T_N = 245 \text{ K}$ for single crystal YbFO.^{14,27} It is reported that the non-stoichiometric samples show a ferrimagnetic and spin-glass transitions at higher temperatures in comparison to the stoichiometric samples.²⁸ This suggests that our sample quality is good. In fact, our magnetization data are very similar and consistent with the data reported by other researchers.^{11,28-30} While LFO goes through a magnetostructural transition at $T_{LT} \sim 175 \text{ K}$,^{8,17} YbFO does not show such transition. The broad peak at 190 K, however, indicates a change in the spin structures as a result of interaction between spins on different Fe sub-lattices and spin fluctuations. Similarly, the moment drops to the lowest value at $\sim 65 \text{ K}$ before starting to increase, suggesting further changes in the spin structures of the system. At low temperature, the spins of Yb^{3+} ions could play a significant role in the magnetic state of the system. In particular, the interactions of the Yb^{3+} ($4f^{13}$) spins with the Fe spins could lead to a complicated spin structure at low temperatures. We interpret that the reversal of the moment below 65 K is due to the emergence of the spins of Yb^{3+} ions.

In order to explore the low-temperature magnetic properties, we measured the temperature dependence of the magnetic moment (M) versus the magnetic field (H)

between 4 K and 300 K, and the representative M-H graphs are shown in Fig. 2(b) and (c). As expected in a ferrimagnetic state, the M-H hysteresis loops were observed only below 243 K. The hysteresis loops show a strong temperature dependence: the M-H loop size in-

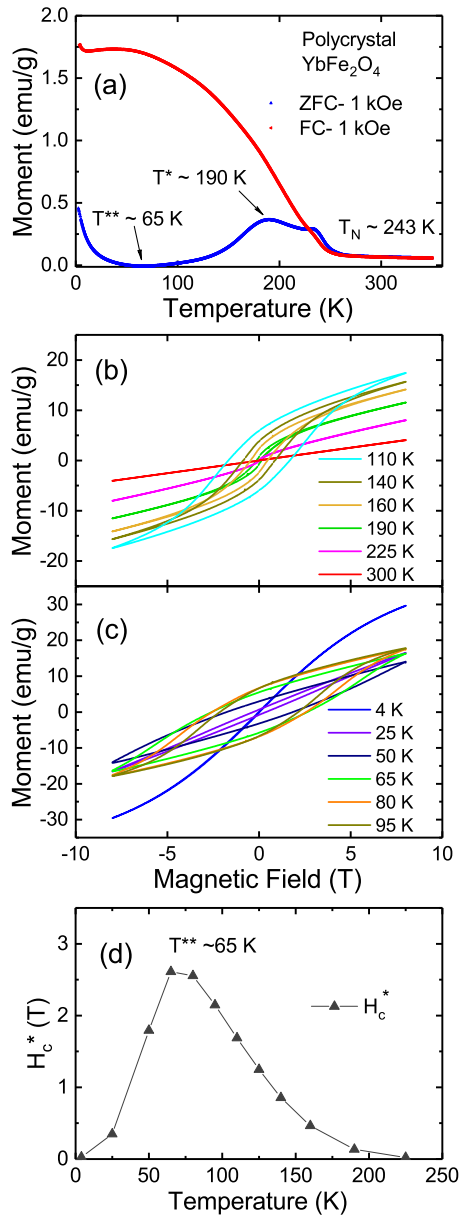


FIG. 2. (a) ZFC and FC magnetic moment versus temperature for a polycrystalline YbFO pellet showing the ferrimagnetic transition temperature at ~ 243 K, followed by the two low-temperature transitions at ~ 190 K and ~ 65 K, respectively. These transitions represent the spin fluctuation effect and a spin-glass transition. Magnetic moment versus the field between (b) 110 K and 300 K and (c) 4 K and 95 K. The M-H hysteresis loops exist below 240 K, with the largest loop area at ~ 65 K, and then the loop starts weakening below 65 K. (d) The coercive field (H_c^*) as a function of temperature, indicating the peak value at ~ 65 K.

creases upon cooling down to ~ 65 K and then decreases rapidly below it. It is noted that the hysteresis loop at 4 K has an S-shape with a small coercivity although the magnetization is not fully saturated within the range of the applied field of 8 T. This behavior can be interpreted as a sign of a spin glass because the spin frustration in the system prevents the frozen moments to fully align in the field direction.³¹ In Figure 2(d), we show the coercive field as a function of temperature, displaying the largest value at $\sim 65 \pm 10$ K. Below 65 K, the coercive field rapidly decreases to almost zero at 4 K. This temperature dependence of the M-H loop offers insight into the magnetic state in YbFO. For a ferrimagnetic state without any competing spin structures, the M-H loop size should gradually increase upon cooling. In contrast, the M-H loops [Fig. 2(b),(c)] show decreasing trend, a strong indication of a complex spin structure below 65 K. While there are no detail M-H hysteresis studies on YbFO, Sun et al.²⁷ have reported the coercive field for single crystal YbFO to be ~ 10 T at 25 K. Based on the observed hysteresis loops, we suggest that the magnetic state of polycrystalline YbFO is no longer ferrimagnetic below 65 K rather it points to a complex magnetic state. It is possible that the observed temperature dependence of the M-H hysteresis loops below 65 K could be attributed to a spin-glass state due to the competition between ferromagnetic and antiferromagnetic interactions of Yb and Fe sub-lattices. There have been reports of a spin-glass state in YbFO below 80 K.^{10,12,13} The one caveat is that the highest magnetic field was 8 T, which was not sufficient to drive the full saturation of magnetization in the sample and thus, the coercive field (H_c^*) value at each temperature (Fig. 2(d)) does not represent its true value and its temperature dependence only represents a qualitative feature. The M-H loop measurements in high magnetic fields ($H > 10$ T) are necessary to find out the true temperature dependence of H_c^* in YbFO.

An ⁵⁷Fe Mössbauer measurement was made at 295 K on the powder YbFO containing 35 mg/cm² of Fe. The spectrum is shown in Fig. 3. The measurement showed that there were two sets of similar electric quadrupole interactions (EQI) but with different isomer shifts (IS). The spectrum was fit with two doublets that had isomer shifts consistent with Fe²⁺ and Fe³⁺ sites. The results were fit with a static quadrupole interaction assuming that the sample was in the low frequency hopping regime where the sample quadrupole interactions were stable relative to the 100 ns Mössbauer time window. The fitting results are shown in the Table. The uncertainty of the fit to the data is indicated in parentheses. The spectrum also showed some small peaks in the high velocity range which indicate that a small amount of impurities Fe₂O₃ and/or Fe₃O₄ were probably present. The xrd analysis shows the presence of a small amount of Fe₂O₃. Because of the small area due to impurities and noise level, the contribution of impurities relative to the main spectrum of YbFO could not be carefully fit and analyzed. Note that the results of the Mössbauer measurement on

Table: Mössbauer parameters (EQI, IS, and Γ) for YbFe_2O_4 at 295 K. The uncertainties are shown in parentheses.

YbFe_2O_4	Fe^{2+}	Fe^{3+}
EQI (mm/s)	0.36 (.10)	0.23 (.10)
IS (mm/s)	1.01 (.10)	0.37 (.10)
Γ (mm/s)	0.40 (.10)	0.40 (.10)

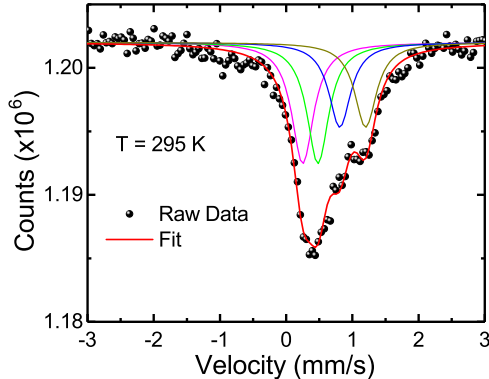


FIG. 3. Room temperature Mössbauer spectrum of YbFO, showing two distinct peaks associated with Fe^{2+} and Fe^{3+} sites. The solid lines represent the fitting to the data.

YbFO are comparable to those of LFO in our previous paper.²³ Other Mössbauer measurements³² on the single crystal LFO that was powdered showed similar experimental results at 295 K as that obtained here for YbFO samples.³² The Mössbauer data on the powdered single crystal were measured from 400 K to 260K and were fit with a Blume-Tjon relaxation model appropriate for a system undergoing fluctuations while our fit was based on a static quadrupole interaction.

We measured resistivity (ρ) of YbFO and the field-induced changes in resistance in the magnetic fields up to ± 8 T. Figure 4(a) shows the resistivity as a function of temperature for a polycrystal YbFO. The resistivity increases by more than five orders of magnitude upon cooling from 300 K to 140 K and the behavior is consistent with an insulating character of YbFO. The resistivity below 140 K, however, was too high to measure with the setup used. Our resistivity data are consistent with the resistivity measured by Blasco et al.¹² In particular, the temperature dependence is strikingly similar, but the resistivity values are slightly higher for our polycrystalline sample. On the other hand, the resistivity of YbFO are about one to two orders of magnitude higher than that of LFO.^{23,34} As shown, an Arrhenius function does not accurately fit the resistivity data. To understand the transport property, we used Mott's variable-range hopping (VRH) conduction model developed for non-crystalline solids with localized charge-carrier states.³³ The inset shows the logarithmic resistivity as a function

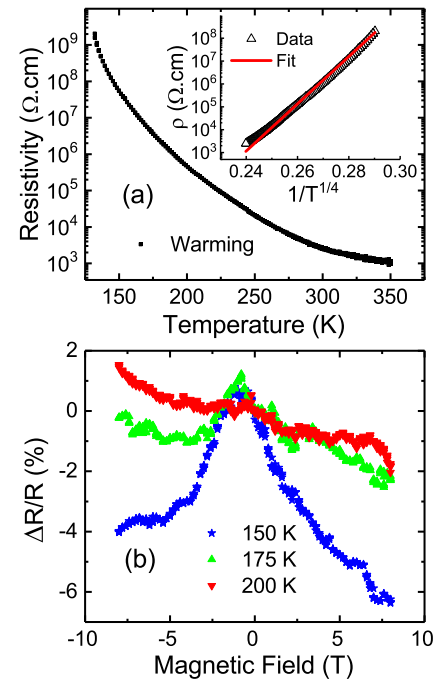


FIG. 4. (a) Resistivity as a function of temperature for a polycrystalline YbFO, showing five orders of magnitude increase from 350 K to 140 K. The inset shows the logarithmic resistivity versus $T^{-1/4}$ graph. The solid line represents the Mott's VRH model fitting to the data. (b) The magnetoresistance ($\Delta R/R$) of a YbFO sample as a function of the magnetic field at three different temperatures. The observed $\Delta R/R$ is up to -6 % and quadratic-field dependent.

of $T^{-1/4}$, showing a linear relationship of a functional form $\ln \rho \propto T^{-1/4}$. The solid line represents the curve fitting to the VRH model, indicating a fairly good agreement between the model and the experimental data. The fitting yields the characteristic temperature, $T_0 \sim 3.2 \times 10^9$ K, which is comparable to that of LFO.^{23,34,35} The fact that the resistivity data of YbFO can be modeled by the VRH model suggests that the electrical transport in YbFO is dominated by the electron hopping between Fe^{2+} and Fe^{3+} in the measured temperature range of 140 - 300 K. The presence of the impurities and oxygen deficiencies in the sample are the sources of the disorders, thus making the sample non-crystalline solid in which the electrical conductivity is dominated by the electron hopping processes.

Figure 4(b) shows the magnetoresistance (MR) effects of YbFO in the magnetic fields up to ± 8 T at 150 K, 175 K, and 200 K, respectively. We define the MR effects as $\Delta R/R = (R_H - R_0)/R_0$, where R_0 and R_H are the sample resistance in zero-field and in the applied field (H), respectively. The MR effects at 200 K are small and show a linear feature while the shape of the MR effects changes at 150 K and 175 K. The MR effects of YbFO were measured up to -6% for ± 8 T field. The observed MR effects are negative below 175 K and independent of the field directions, suggesting that the applied field

suppresses the resistance and the effects are quadratic field dependent. Note that there is a small asymmetry in the MR effects, which is likely caused by the hysteresis effect. As we measured the MR effects by sweeping the field from +8 T to -8 T, after each scan the zero-field resistance changed from its previous value, suggesting a hysteresis effect. Given the dominance of the Fe^{2+} - Fe^{3+} electron hopping processes in the electrical conduction of YbFO, we interpret the observed MR effects as the field-induced modifications of such electron hopping processes. In particular, when the field is applied, the spin-polarized electron tunneling through the grain boundaries and the field-dependent charge hopping between Fe^{2+} and Fe^{3+} sites are expected to increase,³⁶⁻³⁸ thus decreasing the sample resistance. In addition, the contribution of the spin-disorder scattering to the resistivity may also play a role in the effects. For instance, when the field is applied, the spin-disorder scattering decreases, consequently contributing to the negative MR effects.

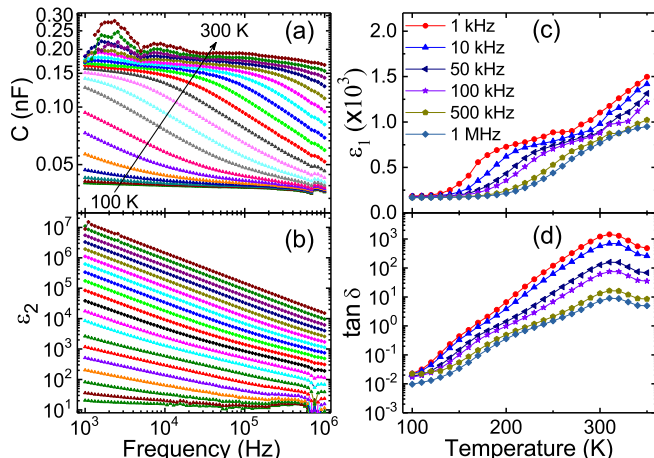


FIG. 5. Frequency dependence of (a) capacitance (C) and (b) the imaginary part (ϵ_2) of the complex dielectric function for a polycrystalline YbFO at temperatures between 100 K and 300 K, in 10 K increments. The imaginary part (ϵ_2) of the dielectric constant gradually decreases as frequency increases without a well defined peak, indicating the influence of extrinsic effects on the response. Temperature dependence of (c) the real part (ϵ_1) and (d) the dielectric loss tangent ($\tan\delta$) of the dielectric function for YbFO at different frequencies measured in the temperature range 100 - 350 K.

Figure 5 (a) and (b) show frequency dependence of the capacitance and the imaginary (ϵ_2) part of the complex dielectric function for a polycrystal YbFO in the temperature range 100 - 300 K, in increments of 10 K. For all the measured temperatures, both capacitance and ϵ_2 decrease gradually over the whole spectrum range. In particular, the low frequency responses are much stronger than the high frequency responses. Moreover, the ϵ_2 spectra do not show a well defined peak associated with the dipolar characteristics of a ferroelectric material. It is noted that none of the reported dielectric responses for YbFO and LFO in literature has a well defined peak in the ϵ_2 spectra.^{10,11,16,18-20,39} Therefore, the observed

frequency dependence in Fig. 5 (b) without a peak in the ϵ_2 spectra is indicative of the presence of the extrinsic effects, which follow the Maxwell-Wagner model. In a sample dominated by the extrinsic effects, $\epsilon_2 \rightarrow \infty$ as frequency $\rightarrow 0$ and $\epsilon_2 \rightarrow 0$ as frequency $\rightarrow \infty$.^{40,41} The possible sources of the extrinsic effects are the grain boundaries, oxygen deficiencies, and the space charge at the electrical contacts.

In Fig. 5 (b) and (c), we show the temperature dependence of the real part (ϵ_1) and the loss tangent ($\tan\delta$) of the dielectric constant for YbFO at frequencies 1 kHz, 10 kHz, 50 kHz, 100 kHz, 500 kHz, and 1 MHz, respectively. The loss tangent clearly indicates a lossy sample, especially in the low frequency region and high temperatures. The room temperature value of ϵ_1 at 1 kHz is ~ 1000 for the YbFO sample. These dielectric spectra fairly compares with the reported dielectric spectra for YbFO.^{10,11,39} Also, these spectra show a typical characteristic: a broad peak in the ϵ_1 spectrum with the peak temperature moving to a higher temperature as the test frequency increases. Such behaviors are interpreted as the signatures of the Maxwell-Wagner effects in the sample.⁴¹ Then, the question arises; what is the intrinsic value of ϵ_1 for YbFO? To estimate the intrinsic value, we need to look at the value of ϵ_1 at low temperature and in the high frequency region where the extrinsic effects on the dielectric constant diminishes. We estimate that the true values for ϵ_1 are on the order of a couple of hundreds, as given by the data at low temperature and high frequencies. Therefore, the observed frequency and temperature dependences of the dielectric constant suggest that the dielectric properties of YbFO were strongly influenced by the contact effects and could not be correlated to ferroelectricity.

Figure 6 (a), (b), and (c) show electric polarization of a YbFO polycrystal pellet as a function of applied electric field at 150 K, 50 K, and 20 K, respectively. The polarization responses of YbFO from room temperature down to 150 K have a shape of an American football (not shown here). The derivative of polarization, which gives a normalized capacitance, has a shape of a letter X, indicating a typical resistive response. The polarization response at 50 K slightly varies from the response at 150 K. Such a polarization response is due to a combination of resistive and dielectric responses. Note that the dielectric behavior of YbFO is masked by the leaky nature of the sample at high temperatures. However, the resistivity of the sample increases significantly below 100 K and thus, the intrinsic dielectric response starts emerging out of the resistive response. This is consistent with the fact that the extrinsic effects on the dielectric properties (Fig. 5) are dominant at high temperatures. Interestingly, the polarization at 20 K is intriguing and at first were thought to indicate ferroelectricity. However, a closer look at the response reveals otherwise. Figure 6 (d) shows the derivative of the polarization data, which has a shape of a letter X rather than a ferroelectric switching behavior, confirming a non-ferroelectric response. There-

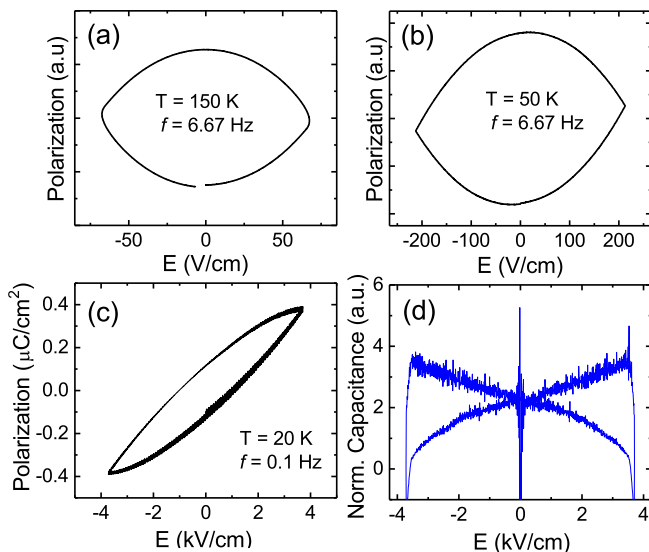


FIG. 6. Electric polarization of YbFO as a function of applied electric field at (a) 150 K (b) 50 K, and (c) 20 K. The polarization responses from 150 K to room temperature have a shape of an American football, indicating a typical resistive response. The polarization as a function of the applied fields at 20 K, appearing as a ferroelectric-like response. (d) The derivative of the polarization at 20 K, however, has a shape of a letter X, confirming a non-ferroelectric response.

fore, the 20 K polarization is still a combination of resistive and dielectric responses. Finally, the polarization data suggest that YbFO is not ferroelectric.

The three-dimensional ferrimagnetic ordering of Fe^{2+} and Fe^{3+} spins in YbFO has been consistent in the samples prepared by various methods. The low temperature magnetic properties of YbFO are interesting and complex due to the emergence of the spin of Yb^{3+} ions and their interactions with the Fe ions. On the other hand, the dielectric and polarization data of YbFO do not unambiguously exhibit ferroelectricity and thus, multiferroicity of YbFO is questionable. So far, the anticipated CO induced ferroelectricity in YbFO and isostructural

LFO has not been observed yet. The disorders and non-stoichiometry due to either iron or oxygen deficiencies in the sample could adversely affect the three dimensional charge ordering from setting in. In other words, the sample quality could be the key to establishing the ferroelectric property of YbFO. Therefore, synthesis of a high quality stoichiometric YbFO sample could help find the answer to whether YbFO is ferroelectric and thus, a multiferroic material.

IV. CONCLUSION

In conclusion, we prepared polycrystalline YbFO samples by an ebeam assisted solid state reaction. The xrd pattern and the ferrimagnetic transition temperature show the single phase YbFO. Mössbauer measurements confirm the two sets of electric quadrupole interactions along with different isomer shifts that are consistent with the presence of Fe^{2+} and Fe^{3+} ions in the sample. The resistivity of YbFO can be fit to the Mott's variable-range hopping conduction model (i.e., $\rho \propto \exp(T_0/T)^{1/4}$). The MR effects of sizes $\sim 6\%$ in the magnetic field of 8 T at 150 K have been observed in the magnetic state. The field-induced changes in the electron hopping between Fe^{2+} and Fe^{3+} could be the mechanism for the MR effects. The coercive field demonstrates a strong temperature dependence with the maximum value at ~ 65 K, possibly indicating a complex spin-glass state below 65 K. The temperature and frequency dependence of the dielectric constant of YbFO can be interpreted as the extrinsic effects. Finally, the electric polarization measurements show no evidence of the intrinsic ferroelectricity in polycrystalline YbFO.

V. ACKNOWLEDGMENTS

Work at SUNY Buffalo State was supported by the National Science Foundation (DMR-1406766).

* rairc@buffalostate.edu

¹ M. Fiebig, T. Lottermoser, D. Meier, and M. Trassin, *Nat. Rev. Mater.* **1**, 16046 (2016).
² T. Jia, Z. Cheng, H. Zhao, and H. Kimura, *Appl. Phys. Rev.* **5**, 021102 (2018).
³ N. A. Spaldin and R. Ramesh, *Nat. Mater.* **18**, 203 (2019).
⁴ N. Ikeda, H. Ohsumi, K. Ohwada, K. Ishii, T. Inami, K. Kakurai, Y. Murakami, K. Yoshii, S. Mori, Y. Horibe, and H. Kito, *Nature* **436**, 1136 (2005).
⁵ A. Nagano, M. Naka, J. Nasu, and S. Ishihara, *Phys. Rev. Lett.* **99**, 217202 (2007).
⁶ Y. Yamada, K. Kitsuda, S. Nohdo, and N. Ikeda, *Phys. Rev. B* **62**, 12167 (2000).
⁷ M. Angst, R. P. Hermann, A. D. Christianson, M. D. Lumsden, C. Lee, M.-H. Whangbo, J.-W. Kim, P. J. Ryan,

S. E. Nagler, W. Tian, R. Jin, B. C. Sales, and D. Mandrus, *Phys. Rev. Lett.* **101**, 227601 (2008).
⁸ A. D. Christianson, M. D. Lumsden, M. Angst, Z. Yamani, W. Tian, R. Jin, E. A. Payzant, S. E. Nagler, B. C. Sales, and D. Mandrus, *Phys. Rev. Lett.* **100**, 107601 (2008).
⁹ Y. Murakami, N. Abe, T. Arima, and D. Shindo, *Phys. Rev. B* **76**, 024109 (2007).
¹⁰ Y. Sun, Y. Liu, F. Ye, S. Chi, Y. Ren, T. Zou, F. Wang, and L. Yan, *J. Appl. Phys.* **111**, 07D902 (2012).
¹¹ K. Yoshii, N. Ikeda, Y. Matsuo, Y. Horibe, and S. Mori, *Phys. Rev. B* **76**, 024423 (2007).
¹² J. Blasco, S. Lafuerza, J. Garcia, and G. Subias, *Phys. Rev. B* **90**, 094119 (2014).
¹³ H. L. Williamson, T. Mueller, M. Angst, and G. Balakrishnan, *J. Cryst. Growth* **475**, 44 (2017).

- ¹⁴ K. Fujiwara, T. Karasudani, K. Kakurai, W. T. Lee, K. C. Rule, A. J. Studer, and N. Ikeda, *J. Phys. Soc. Jpn.* **88**, 044701 (2019).
- ¹⁵ N. Ikeda, *J. Phys.: Condens. Matter* **20**, 434218 (2008).
- ¹⁶ J. de Groot, T. Mueller, R. A. Rosenberg, D. J. Keavney, Z. Islam, J. W. Kim, and M. Angst, *Phys. Rev. Lett.* **108**, 187601 (2012).
- ¹⁷ J. de Groot, K. Marty, M. D. Lumsden, A. D. Christianson, S. E. Nagler, S. Adiga, W. J. H. Borghols, K. Schmalzl, Z. Yamani, S. R. Bland, R. de Souza, U. Staub, W. Schweika, Y. Su, and M. Angst, *Phys. Rev. Lett.* **108**, 037206 (2012).
- ¹⁸ P. Ren, Z. Yang, W. Zhu, C. Huan, and L. Wang, *J. Appl. Phys.* **109**, 074109 (2011).
- ¹⁹ D. Niermann, F. Waschkowski, J. de Groot, M. Angst, and J. Hemberger, *Phys. Rev. Lett.* **109**, 016405 (2012).
- ²⁰ A. Ruff, S. Krohns, F. Schrettle, V. Tsurkan, P. Lunkenheimer, and A. Loidl, *Eur. Phys. J. B* **85**, 1 (2012).
- ²¹ A. J. Hearmon, D. Prabhakaran, H. Nowell, F. Fabrizi, M. J. Gutmann, and P. G. Radaelli, *Phys. Rev. B* **85**, 014115 (2012).
- ²² T. Nagata, P.-E. Janolin, M. Fukunaga, B. Roman, K. Fujiwara, H. Kimura, J.-M. Kiat, and N. Ikeda, *Appl. Phys. Lett.* **110**, 052901 (2017).
- ²³ R. C. Rai, J. Pawlak, J. Hinz, M. Pascolini, and M. DeMarco, *J. Appl. Phys.* **124**, 144101 (2018), <https://doi.org/10.1063/1.5042514>.
- ²⁴ K. Kato, I. Kawada, N. Kimizuka, and T. Katsura, *Zeitschrift Fur Kristallographie* **141**, 314 (1975).
- ²⁵ R. Blake, R. Hessevick, T. Zoltai, and L. W. Finger, *American Mineralogist: Journal of Earth and Planetary Materials* **51**, 123 (1966).
- ²⁶ M. Marezio, J. Remeika, and P. Dernier, *Acta Crystallographica Section B: Structural Crystallography and Crystal Chemistry* **26**, 2008 (1970).
- ²⁷ Y. Sun, J.-Z. Cong, Y.-S. Chai, L.-Q. Yan, Y.-L. Zhao, S.-G. Wang, W. Ning, and Y.-H. Zhang, *Appl. Phys. Lett.* **102**, 172406 (2013).
- ²⁸ H. Kobayashi, K. Fujiwara, N. Kobayashi, T. Ogawa, M. Sakai, M. Tsujimoto, O. Seri, S. Mori, and N. Ikeda, *J. Phys. Chem. Solids* **103**, 103 (2017).
- ²⁹ K. Yoshii, D. Matsumura, H. Saitoh, T. Kambe, M. Fukunaga, Y. Muraoka, N. Ikeda, and S. Mori, *J. Phys. Soc. Jpn.* **83**, 063708 (2014).
- ³⁰ K. Fujiwara, M. Miyajima, M. Fukunaga, J. Kano, H. Kobayashi, and N. Ikeda, *Trans. Mat. Res. Soc. Jpn.* **41**, 139 (2016).
- ³¹ K. Binder and A. P. Young, *Rev. Mod. Phys.* **58**, 801 (1986).
- ³² X. S. Xu, M. Angst, T. V. Brinzari, R. P. Hermann, J. L. Musfeldt, A. D. Christianson, D. Mandrus, B. C. Sales, S. McGill, J. W. Kim, and Z. Islam, *Phys. Rev. Lett.* **101**, 227602 (2008).
- ³³ N. F. Mott, *J. Non-Crystal. Solids* **1**, 1 (1968).
- ³⁴ B. Fisher, J. Genossar, L. Patlagan, and G. M. Reisner, *J. Appl. Phys.* **109**, 084111 (2011).
- ³⁵ S. Lafuerza, J. Garcia, G. Subias, J. Blasco, K. Conder, and E. Pomjakushina, *Phys. Rev. B* **88**, 085130 (2013).
- ³⁶ G. Q. Gong, A. Gupta, G. Xiao, W. Qian, and V. P. Dravid, *Phys. Rev. B* **56**, 5096 (1997).
- ³⁷ W. Eerenstein, T. T. M. Palstra, S. S. Saxena, and T. Hibma, *Phys. Rev. Lett.* **88**, 247204 (2002).
- ³⁸ C. Park, Y. Peng, J. G. Zhu, D. E. Laughlin, and R. M. White, *J. Appl. Phys.* **97**, 10C303 (2005).
- ³⁹ Y. Liu, T. Zou, F. Wang, X.-Q. Zhang, Z.-H. Cheng, and Y. Sun, *Phys. B-Condensed Matter* **405**, 3391 (2010).
- ⁴⁰ P. Lunkenheimer, V. Bobnar, A. V. Pronin, A. I. Ritus, A. A. Volkov, and A. Loidl, *Phys. Rev. B* **66**, 052105 (2002).
- ⁴¹ G. Catalan, D. O'Neill, R. M. Bowman, and J. M. Gregg, *Appl. Phys. Lett.* **77**, 3078 (2000).